Sensors and Actuators Reports 4 (2022) 100097

Contents lists available at ScienceDirect

Sensors and Actuators Reports

journal homepage: www.sciencedirect.com/journal/sensors-and-actuators-reports

Stripping voltammetry and chemometrics assisted ultra-selective, simultaneous detection of trace amounts of heavy metal ions in aqua and blood serum samples

Lignesh Durai, Sushmee Badhulika *

Department of Electrical Engineering, Indian Institute of Technology, Hyderabad 502285, India

ARTICLE INFO

Keywords:
Al_2NiCoO_5
Electrochemical sensor
Heavy metal ions detection
Simulated blood serum
Principal component analysis (PCA) analysis

ABSTRACT

We present a one-step, solid-state synthesis of Al_2NiCoO_5 nanoflakes (ANC) modified glassy carbon electrode (GCE) for ultra-selective and trace level simultaneous detection of HMIs like copper (Cu^{2+}), mercury (Hg^{2+}), cadmium (Cd^{2+}), and lead (Pb^{2+}) ions in aqua and simulated blood serum samples. ANC/GCE sensor exhibits a low limit of detection (LOD = 3S/m) of 0.00154 ppb, 0.00232 ppb, 0.00261 ppb and 0.00114 ppb towards Pb^{2+}, Hg^{2+} Cu^{2+} and Cd^{2+} ions, correspondingly that are far lower than the perilous limits of HMI concentration reported for blood serum and water samples. The quantitative study and multiple response analysis of the sensor towards each metal ions are accomplished via principal component analysis (PCA) which verifies the selectivity of the ANC/GCE sensor with satisfactory recovery percentages. The superior performance, reproducibility and stability of the sensor are attributed to the electrocatalytic active sites of ANC nanoflakes facilitated by the Ni^{2+}/Ni^{3+} and Co^{2+}/Co^{3+} redox couple along with the oxy-functional groups. The sensor was efficacious in detecting the trace level concentrations of HMIs in samples like simulated blood serum, drinking water and tap water with good recovery percentages. This efficiency of the sensor demonstrates it as a promising platform for a broad-spectrum of environmental and bioanalytical applications.

1. Introduction

Heavy metals i.e., metals with a specific density greater than 5 g/cm^3, play a vital role in the metabolic functions of living organisms at trace level concentrations and recognized as lethal at higher concentrations [1,2]. Among the range of heavy metals found in the environment lead, cadmium, copper, arsenic, mercury, chromium, nickel, and zinc are known as the noxious heavy metals that have severe adverse health effects [1,2]. The standard physiological concentration of lead in the human body is 50 ppb, above which it can cause neurological disorders like attention discrepancy, hyperactivity syndrome, inferior birthweight etc [3]. Likewise, the excessive concentration of cadmium (normal physiological concentration; 5 ppb) mercury (normal physiological concentration; 0.2 ppb) in human blood can lead to various types of cancer such as breast, pancreas, kidney cancers and harm directly harms systems like the nervous, digestive, the immune system of the human body, respectively [4,5]. In contrast, the low concentration of copper below 100 ppb (normal physiological range 100 ppb to 150 ppb) can be associated with kidney disease, nutritional deficiency, and inability to absorb copper while the higher concentration above 150 ppb can cause liver diseases, under reactive thyroid leukaemia, lymphoma, rheumatoid arthritis etc. [6]. Generally, these heavy metals ion (HMIs) easily accumulated into the human physiological system via the consumption of contaminated water and foods [7]. In the past few decades, a wide range of analytical techniques have been reported for the detection of HMIs in blood and water samples like atomic fluorescence spectroscopy, inductively coupled plasma-mass spectroscopy (ICP-MS), X-ray fluorescence spectroscopy, inductively coupled plasma atomic emission spectroscopy (ICP-AES) and electrochemical analysis [8,9]. However, these analytical techniques involve time-consuming procedures and expensive equipment this making them inapt for portable and *in-situ* analysis. The electrochemical analysis provides a low-cost and rapid platform for HMI detection in water and blood samples but, the coexistence of different HMIs at trace level concentrations in human blood and water bodies requires a highly stable and selective technique. The inevitability of the simultaneous sensing of HMIs has attracted significant attention [8]. Chemically modified electrodes are cost-effective and portable with the facile fabrication process, high

* Corresponding author.
E-mail address: sbadh@iith.ac.in (S. Badhulika).

https://doi.org/10.1016/j.snr.2022.100097
Received 14 November 2021; Received in revised form 16 February 2022; Accepted 27 March 2022
Available online 8 April 2022

stability, sensitivity, and selectivity via anodic stripping voltammetry (ASV) [9], square-wave anodic stripping voltammetry (SWASV) [10], etc. Hu et al. reported a copper-based metal−organic framework (HKUST-1) modified GCE as an electrochemical sensor for the detection of Pb^{2+} and Cd^{2+} ions in water samples [11]. Malik et al. reported zinc oxide-decorated multiwalled carbon nanotubes modified GCE for electrochemical sensing of Pb^{2+} ions [12]. Huo et al. demonstrated an amino-functionalized MOF (3DGO/UiO-66-NH_2) based electrochemical sensor for simultaneous sensing of HMIs [13]. Though these sensors reported simultaneous detection of HMIs with complex fabrication techniques and they failed to provide high chemical stability and reliability.

In recent years, perovskite materials have attracted significant interest for sensing due to their high mechanical stability, facile synthesis, and electrocatalytic active sites [8]. Among the lead-free perovskites, Al_2NiCoO_5 (ANC) is the least studied double perovskite material with an $A_2BB'O_5$ structure. Owing to their high mechanical stability and energy density, double perovskites have been widely studied for energy storage applications [14]. There are numerous reports on the efficacious synthesis of double perovskite materials via conventional wet-chemical synthesis techniques like sol-gel, co-precipitation, hydrothermal, etc. [15]. Though these techniques provide control over the size, geomorphology of the material, they require expensive precursors and result in low yield. To overcome limitations and obtain excellent purity and chemical homogeneity, direct solid-state reaction-assisted synthesis is preferred.

Principal component analysis (PCA) is one of the reliable multiple response statistical analysis techniques that reduce the dimensionality in large datasets and improve the interpretability through smaller sets of summary indices which can be more easily analyzed and visualized by persevering as much variability as possible [16]. Generally, PCA generates a linear combination of the original variables to generate the axes which are known as principal components (PCs), which reduces to solving an eigenvalue or eigenvector problem [17]. Besides, the adaptability of the PCA technique has made it more interesting and significantly useful for a wide variety of datasetslike binary, ordinal, compositional, discrete and symbolic from various disciplines [18]. The major advantages of the PCA over other statistical analysis techniques are as follows, (1) deficiency in data is given thru orthogonal components, (2) elimination of correlated variables which don't contribute towards decision making, (3) disabling data overfitting issues by reducing the number of features, (4) high variance and (5) improved visualization with minimized noise data [17–19]. Hence, the PCA technique was used in this work for the data visualization process and to confirm the spanned scatter plot distributions of the chronicled sensor response towards HMIs.

Here, we present a novel, one-step, solid-state reaction-assisted synthesis of ANC nanoflakes for simultaneous sensing of copper (Cu^{2+}), lead (Pb^{2+}), mercury (Hg^{2+}), and cadmium (Cd^{2+}) in water and simulated blood serum samples. The ANC modified GCE (ANC/GCE) sensor displayed an outstanding selectivity, sensitivity, and stability towards simultaneous sensing of HMIs via anodic stripping differential pulse voltammetry analysis (ASDPV). The overall efficacy of the ANC/GCE sensor towards HMI detecetion can be accredited to the high electrocatalytic property of the ANC nanoflakes which is enabled with Ni^{2+}/Ni^{3+} and Co^{2+}/Co^{3+} redox couples and oxy functional groups at their surface. To the best of our acquaintance, this is the first report on the ANC nanoflakes for the versatility of application in the trace-level determination of HMIs in biofluids (i.e., simulated blood serum) and aqua (i.e., drinking and tap water) samples.

2. Experimental

2.1. Materials

The chemical like Aluminium oxide (Al_2O_3, 99.9%), Mercury nitrate ($Hg(NO_3)_2$, 99.9%), Nickel oxide (NiO, 99.9%), Cobalt oxide (CoO, 99.9%), Copper nitrate ($Cu(NO_3)_2$, 99.9%), Cobalt nitrate ($Co(NO_3)_2$, 99.9%) and ethanol (99.9%) were acquired from Sigma Aldrich. DI water with 18 MΩ.cm was obtained from the Millipore system.

2.2. Synthesis of ANC nanoflakes

The solid state synthesis of ANC nanoflakes was perfomed as reported in a recent work from our lab [21]. In brief, the stoichiometric measure of Al_2O_3, CoO, and NiO was grounded using mortar and pestle. The obtained powder was then reacted at 950 °C for 24 h with 30 °C/min as the ramping temperature using a muffle furnace. The end product was naturally cooled and grounded. to a fine powder. The overall chemical reaction is given in Eq. (1)

$$NiO + CoO + Al_2O_3 \rightarrow Al_2NiCoO_5 \quad (1)$$

2.3. Sensor fabrication

Generally, the fabrication of chemically modified GCE is achieved via the drop-casting technique. Here the obtained fine powder of ANC is homogenously dispersed via ultrasonication (30 min) in dimethylformamide (DMF) solution at room temperature. The 6 µL of the resultant solution was drop cast onto the cleaned and polished GCE electrode and dried at 70 °C in a hot air oven for 10 m. Finally, the dried ANC/GCE was used for all successive electrochemical measurement and simultaneous detection of HMIs

2.4. Physicochemical analysis

The surface morphology and the crystalline structure of the as-synthesized ANC nanoflakes was achieved via field emission scanning electron microscope (FESEM) from Zeiss (model: Zeiss Ultra-55) and X-ray diffraction (XRD) from lineon X'pert PRO X-ray diffractometer (Source: Cu-Kα). The chemical bonding of theANC nanoflakes and their vibrational modes were analyzed via Raman spectra obtained form Wi-Tech Alpha 600 confocal Raman spectrometer (wavelength of the laser source: λ = 532 nm). The presence of different surface functional elements were studied via Fourier Transform Infra-Red (FTIR) spectra collected from IRAffinity spectrophotometer.

2.5. Electrochemical studies of ANC/GCE electrode

The entire electrochemical studies of as-fabricated ANC/GCE sensor was achieved via a three-electrode setup commissioning ANC/GCE as the working electrode, Ag|AgCl electrode in 1M KCl as a reference electrode and Pt wire electrode as the counter electrode connected to CHI 660E (an electrochemical work station from CH Instruments).

The electrochemical active surface area (EASA) of the ANC/GCE electrode was evaluated using cyclic voltammetry (CV) technique in presence of 1 M KCl containing 5 mM of Fe $(CN)_6^{3-/4-}$ electrolytic solution. The EASA was assessed via Randle-Sevik equation, given as Eq. (2).

$$i_{pa} or i_{pc} = 2.69 \times 10^5 \times A_e \times D^{\frac{1}{2}} \times n^{\frac{3}{2}} \times v^{\frac{1}{2}} \times c \quad (2)$$

where, A_e is the effective surface area of the electrode, D is the diffusion coefficient (i.e., $D = 7.6 \times 10^{-6}$ cm^2/s), n is the number of electrons, and c is the concentration (mol/cm^3) of redox probe and υ is the scan rate of the cyclic voltammetry analysis performed (i.e., 10 mV/s,),

The chronocoulometric analysis of ANC/GCE was performed to obtain the active surface coverage area (Γ) of reactant ions from the electrolyte. The Γ was estimated employing Eq. (3).

$$Q = nFA\Gamma \quad (3)$$

Where Γ is the active surface coverage area, n is the number of transferred electrons, F is the faraday constant, Q is the variance between reverse and forward intercepts and A is the active area of electrode (i.e., 0.0707 cm^2). The induviual and simultaneous detection of HMIs were performed via anodic stripping differential pulse voltammetry (ASDPV) technique in presence of acetate buffer solution (0.1 M ABS) with optimized pH value.

3. Results and discussion

The detailed physiochemical analysis of the as-fabricated ANC nanoflakes is provided in the supplementary information (SI).

3.1. Electrochemical study

The electrocatalytic characteristics of the ANC nanoflakes modified GCE (ANC/GCE) were examined via cyclic voltammetry (CV) analysis in the presence of 5 mM Fe $(CN)_6^{3-/4-}$ redox probe with 1 M KCl with a scan rate of 10 mV/s. Fig. S3 (a) shows the characteristic CV analysis of bare GCE and ANC/GCE. Noteworthy, that the increase in the redox peak current (I_p) was more significant than the unmodified GCE. The intensification in the Ip was accredited to the excellent electrocatalytic activity of the ANC nanoflakes facilitated with the Ni^{2+}/Ni^{3+} and Co^{2+}/Co^{3+} redox couples at the octahedra sites. In addition to the electrocatalytic activity of the ANC nanoflakes the oxy functional surface groups, significantly contribute towards the redox reaction of Fe^{3+}/Fe^{4+} present in the Fe $(CN)_6^{3-/4-}$ redox probe [8]. The EASA of the ANC/GCE was calculated as 0.698 cm^2 (i.e., ~119.89% larger than the bare GCE (0.175 cm^2)). This increase in the EASA was ascribed to the existence of electrocatalytic sites in the ANC nanoflakes. The peak potential separation (ΔE_p), (i.e., the difference between the cathodic and anodic peak potentials) was appraised as 80 mV (vs Ag|AgCl) that is inferior to the bare GCE (i.e., 98 mV (vs Ag|AgCl)). This reduction in the ΔE_p can be ascribed to the faster electron transfer mechanism at the surface of the ANC/GCE electrode than the bare GCE. Fig. S3 (b) illustrates the chrono-coulometry analysis of the GCE and ANC/GCE. The sensor was estimated with an active surface coverage (Γ) of 8.68 nmol cm^{-2} (i.e., 180% greater than bare GCE). This substantial agumentation in the Γ was accredited to the presence of abundant OH functional groups at the surface of ANC nanoflakes [20].

3.2. Optimization studies

The four major conditions that impact the sensitivity and stability of any surface modified electrode for HMI detection are (i) the loading of active material (wt.%), (ii) the pH of the electrolyte used, (iii) deposition voltage and (iv) deposition time. These parameters were optimized for the as-fabricated ANC/GCE sensor to acquire the maximum efficacy towards trace level detection of HMIs in ecological and biological fluids.

3.2.1. Effect of Wt.%

In this process of optimizing the wt.% of the active material ANC nanoflakes (such as 0.1, 0.3, 0.5, 0.7, and 0.9 wt.%.), the ASDPV response of the sensor towards equimolar concentration of 0.05 ppb Cu^{2+}, Hg^{2+}, $Pb^{2+,}$ and Cd^{2+} were analyzed. Fig. S4 (a) shows the performance comparison chart of ANC/GCE sensors at different wt.% towards targetted HMIs in presence of 0.1M ABS electrolytic solution. The maximum retort of the ANC/GCE sensor towards targeted analytes was pragmatic at 0.7 wt.% of ANC modified GCE sensor. This behavior of the electrode was accredited to the optimal obtainability of catalytic active sites facilitating the redox mechanism of the HMIs in the redox probe. The realtively low performance observed overhead 0.7 wt.% was attributed to the disproportionate concentration gradient at the electrode-electrolyte interface due to the high electronegativity of the active material which disturbs the average diffusion length in the electrolytic medium. On the other hand, the dearth of active sites leads to the comparatively low performance of the sensor at wt.% below 0.7.

3.2.2. Effect of pH

The pH of the electrolytic solution has a significant impact on the sensitivity and overall performance of an electrochemical sensor. Fig. S4 (b) shows the performance comparison of the ANC/GCE sensor depending on ASDPV response towards equimolar concentration of 0.05 ppb Cu^{2+}, Hg^{2+}, Pb^{2+} and Cd^{2+} at different pH of supporting electrolytic solutions ranging from 3 pH to 6 pH. The sensor exhibited maximum sensitivity at pH 4.5 than other pH levels of the supporting electrolyte (i.e., 0.1 M ABS) owing to the excellent electrostatic attraction between HMIs and the electrode surface followed by the mechanism of complexation. In addition to the above description, ANC/GCE at 4.5 pH has a curtailed effect of OH^- ions towards the targeted HMIs with an optimum level of H^+ ions [21]. The discrepancy in the performance of the sensor towards HMIs at a higher pH level was accredited to the excessive influence of OH^- ions surrounding the HMIs which is known as the hydrolysis process of HMIs [8]. In contrast, the performance degradation of the ANC/GCE at low pH levels was ascribed to the presence of excessive H^+ cations in the electrolyte which reduces the diffusion length and sensitivity with overall performance of the sensor [21].

3.2.3. Effect of deposition voltage

ASDPV relies on two major mechanisms (i) deposition of metal ions onto the electrode surface and (ii) stripping where the deposited metal ions are oxidized into the electrolytic medium. As the deposition mechanism of HMIs plays a crucial role the voltage used for the process should be optimized to obtain maximum sensitivity. Performance comparison of the sensor towards 0.05 ppb equimolar concentration of Cu^{2+}, Hg^{2+}, $Pb^{2+,}$ and Cd^{2+} via ASDPV technique in presence of 4.5 pH 0.1 M ABS with a deposition time of 25 s at different deposition voltages (i.e., -0.8 to -1.4 V) is as shown in Fig. S3(c). Though the sensor responded at all deposition potential the maximum response was recorded at -1.2 V. This characteristic was ascribed to the unique standard potentials of HMIs. Decisively, -1.2 V was employed as the deposition potential of the ANC/GCE sensor in all upcoming HMI detections using the ASDPV technique.

3.2.4. Effect of deposition time

The deposition time of the sensor using the ASDPV techniques impacts the performance and stability of the sensor towards HMI detection. Fig. S3 (d) depicts the ASDPV performance comparison of ANC/GCE towards 0.05 ppb equimolar concentration of Cu^{2+}, Pb^{2+}, Hg^{2+} and Cd^{2+} at different deposition times from 15 to 35 s and the deposition voltage of -1.2 V. The maximum performance of ANC/GCE sensor towards HMIs is evident at 25 s while the deterioration in sensor response was observed at lower and higher deposition periods. This can be owed to the deficiency of HMI deposition at the electrode surface at a short deposition period and surface saturation of the sensor at a longer deposition period which would shield the electrocatalytic active sites of ANC nanoflakes from accommodating more HMIs [22].

3.3. Electrochemical sensing of HMIs

Convincingly, the optimized parameters of 0.7 wt.% ANC/GCE sensor in presence of 4.5 pH 0.1 M ABS electrolyte with -1.2 V deposition potential and 25 s deposition time was employed for all successive electrochemical sensing of HMIs using ASDPV analysis.

3.3.1. Electrochemical sensing of HMIs – individual

Initially to understand the sensing ability of the sensor towards each HMIs was analyzed via ASDPV in presence of individual HMI. Fig. 1(a) depicts the ASDPV curve of ANC/GCE towards a range of Cd^{2+} concentrations (ranging from 0.01 to 1000 ppb). The distinctive peak

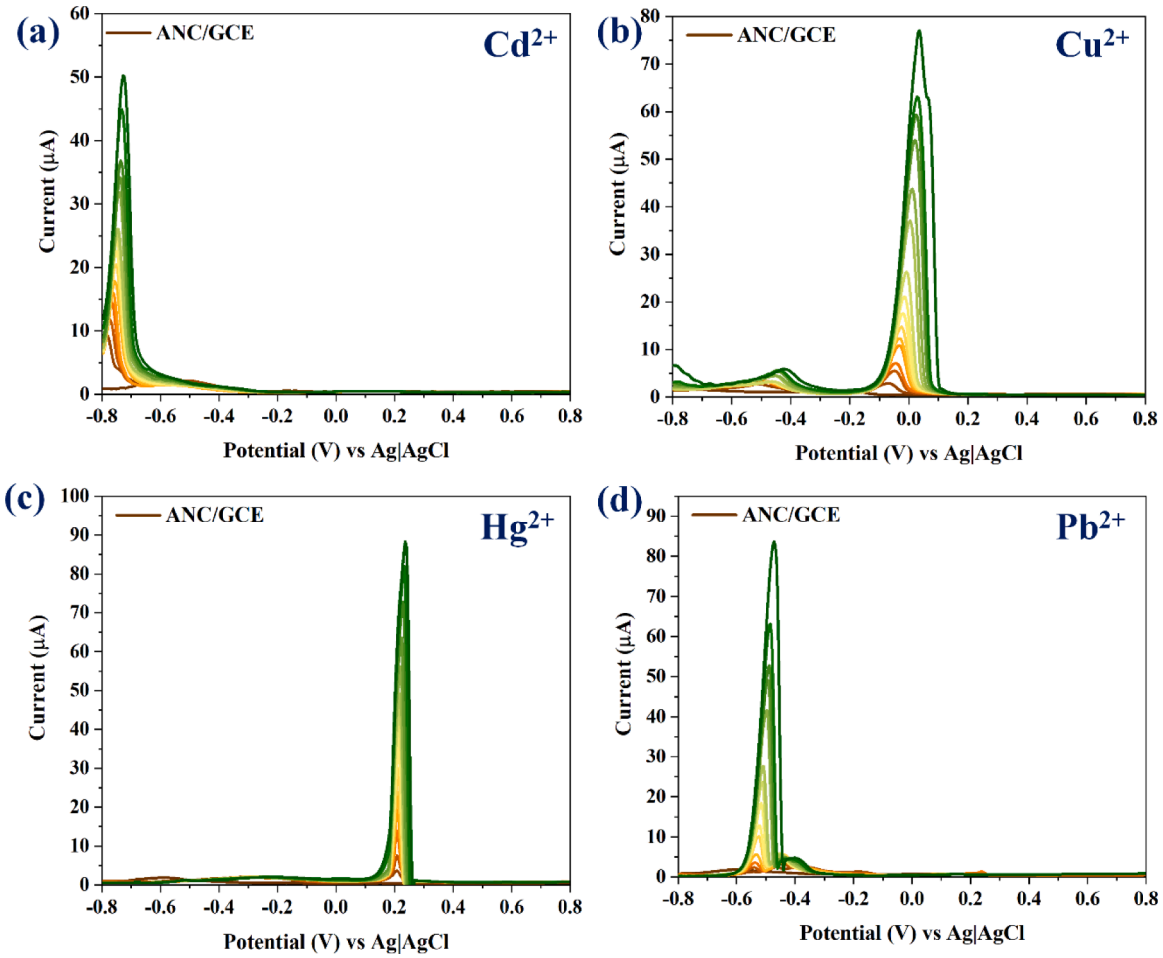

Fig. 1. ASDPV response of ANC/GCE towards (a) Cd^{2+}, (b) Cu^{2+}, (c) Hg^{2+} and (d) Pb^{2+} at concentrations ranging from 0.01 ppb to 1000 ppb.

pragmatic at -0.71 V (vs Ag|AgCl) was ascribed to the oxidation of Cd^{2+} ions from the electrode surface during the striping phase of the proposed ASDPV technique. As the concentration was increased a surge in the oxidation peak current was experiential with an inconsequential peak shift. This augmentation in the oxidation peak current was attributed to the amount of deposited Cd^{2+} ions and their electro-oxidation reaction during the stripping phase of the mechanism. The shift in the peak potential was due to the polarization effect at the electrode surface. The calibration curve obtained for ANC/GCE concerning the response towards Cd^{2+} ions is shown in Fig. S5(a). The limit of detection (LOD = 3S/m, the signal to noise ratio is 3, S is the standard deviation, and m is the slope value of the linear calibration curve) of electrode towards Cd^{2+} was estimated as 0.00114 ppb. The sensitivity of the sensor was calculated as 10.68 μA ppb^{-1} cm^{-2}. Similarly, the sensing ability of the sensor towards the variable concentration of Cu^{2+}, $Hg^{2+,}$ and Pb^{2+} were examined individually via ASDPV analysis as shown in Fig. 1(b), 1(c), and 1(d), respectively. The minor peak observed from -0.4 to -0.6 V(vs Ag|AgCl) for Cu^{2+} (Fig. 1(b)) and Pb^{2+}ions (Fig. 1(d)) can be attributed to the electrochemical reduction of nitrate (NO_3^-) to ammonium (NH_4^-) [23] as shown in Eq. (4).

$$NO_3^- + 10\,H^+ + 8e^- \rightarrow NH_4^- + 3H_2O \quad (4)$$

However, this reduction process of the nitrate anions does not have a significant impact on the sensor response towards the detection of targeted HMIs. Though the sensor exhibits a minor response at -0.4 to -0.6 V(vs Ag|AgCl) for all HMIs in this analysis, the current exhibited was negligible. Hence the peak was not visible in the obtained ASDPV curve shown in Fig. 1(a) and (c). In contrast, the nitrate reduction peak was observed as an additional peak with the ions during the stripping mechanism of ASDPV for Pb^{2+} and Cu^{2+} which can be due to its stripping potential and the high sensitivity of the sensor towards the cations than the anions (nitrate ions).

The sensor exhibited a stable response towards individual HMIs at different oxidation potentials such as -0.07 V (vs Ag|AgCl) for Cu^{2+}, 0. 208 V (vs Ag|AgCl) for Hg^{2+} and -0.536 V (Ag|AgCl) for Pb^{2+} ions. The calibration curves obtained for the ANC/GCE sensor towards individual sensing of Cu^{2+}, $Hg^{2+,}$ and Pb^{2+} are illustrated in Fig. S5 (b), (c) and (d) respectively. The LOD of the sensor towards Cu^{2+}, Hg^{2+}, and Pb^{2+} was appraised as 0.00261, 0.00232, and 0.00154 ppb, respectively. The sensor displayed a sensitivity of 20.34 , 23.85 and 22.92 μA ppb^{-1} cm^{-2} towards Cu^{2+}, Hg^{2+} and Pb^{2+} ions, respectively.

3.3.2. *Electrochemical sensing of HMIs – simultaneous*

The simultaneous sensing of the Cu^{2+}, Hg^{2+}, Cd^{2+}, and Pb^{2+} was performed via the ASDPV technique with optimized parameters in the existence of 0.1 M ABS (pH 4.5) electrolytic solution. Fig. 2(a) depicts the ASDPV curve with variable HMI concentrations from 0.01 to 10 ppb. The conventional sensing process of the HMI detection using the ASDPV technique consists of two key phases such as deposition and stripping as shown in Fig. 2(b). In the deposition phase of the process, the metal ions get reduced (like Cu^0, Hg^0, Pb^0, and Cd^0) and deposited onto the electrode surface. Later in the stripping process, as the voltage was swept from lower potential to higher potential (i.e., from -0.8 to +0.8), the deposited HMIs gets oxidized into the electrolytic medium at different oxidation potentials. This can be ascribed to the key aspect that favored the simultaneous sensing of HMIs, i.e., the standard oxidation potentials of the metals.

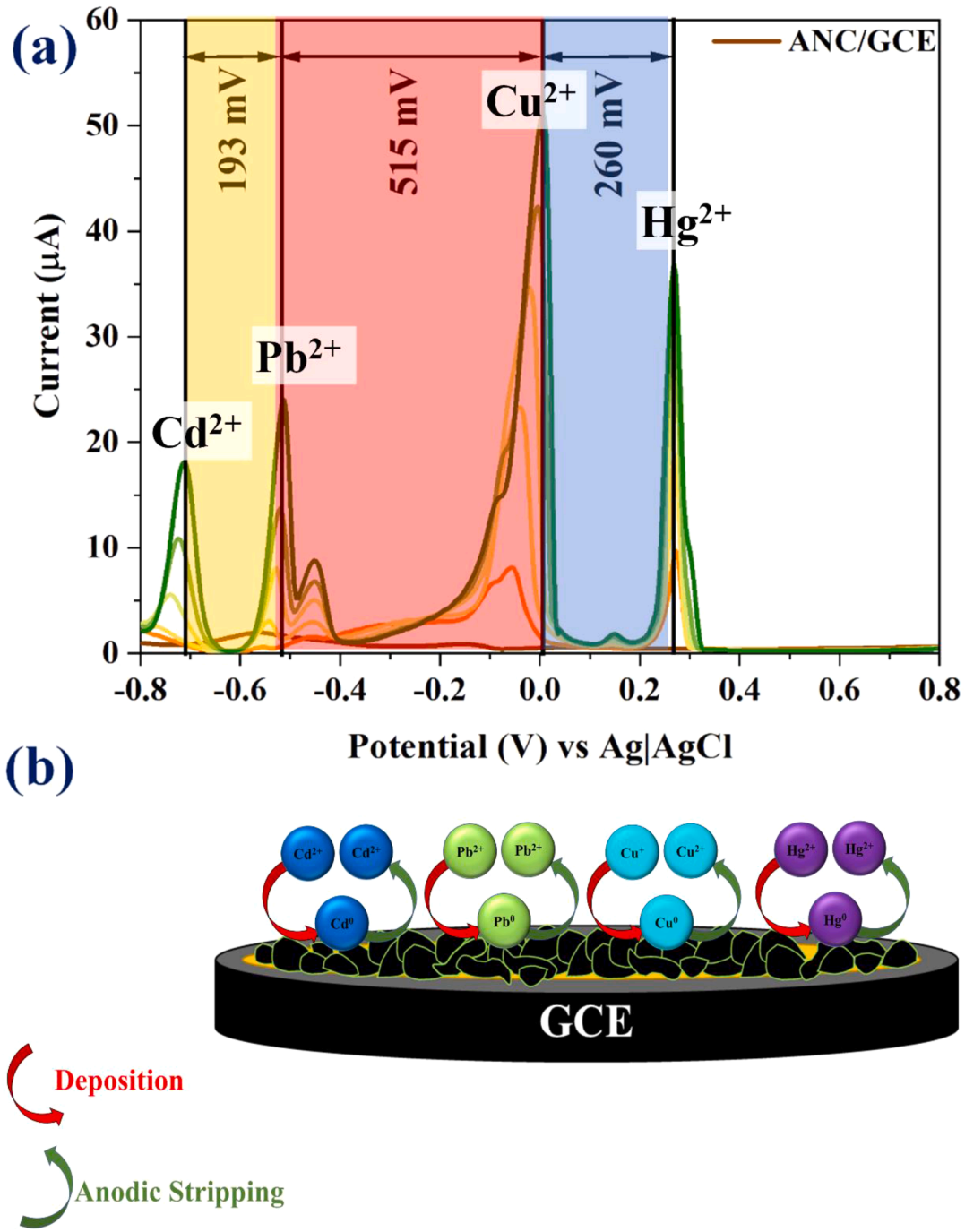

Fig. 2. (a) the simultaneous ASDPV response of ANC/GCE towards Cd^{2+}, Cu^{2+}, Hg^{2+} and Pb^{2+} with concentrations ranging from 0.01 ppb to 10 ppb (c) HMI sensing mechanism of ANC/GCE sensor.

The peak-to-peak separation (ΔE_P) of ANC/GCE in simultaneous detection of HMIs was observed as 193 mV (between Cd^{2+} and Pb^{2+}), 515 mV (between Pb^{2+} and Cu^{2+}), and 260 mV (between Cu^{2+} and Hg^{2+}). This proves the efficacy and simultaneous sensing ability of the ANC/GCE sensor. The calibration curve corresponding to the ASDPV response of the ANC/GCED sensor with the linear regression line is shown in Fig. S6 (a–d). The sensor was estimated with a LOD of 0.00094 ppb (Cd^{2+}), 0.00105 ppb (Pb^{2+}), 0.00121 ppb (Cu^{2+}), and 0.00198 ppb (Hg^{2+}). The sensitivity was calculated as 22.99 μA ppb^{-1} cm^{-2} (Cd^{2+}), 32.70 μA ppb^{-1} cm^{-2} (Pb^{2+}), 60.18 μA ppb^{-1} cm^{-2} (Cu^{2+}) and 30.31 μA ppb^{-1} cm^{-2} (Hg^{2+}). Comparing the response of ANC/GCE sensor to individual HMIs, the simultaneous detection exhibits low LOD and high sensitivity which can be attributed to the intermetallic compound formation (such as Pb-Hg) at the electrode surface. This contributes towards the augmentation in the sensitivity of the sensor towards other HMIs. The reliability of the simultaneous sensing of HMIs via CV analysis was examined as shown in Fig. S7. The ΔE_P observed has a good agreement with ASDPV analysis proving the efficacy of the sensor. This outstanding Performance of the ANC/GCE can be accredited to the electrocatalytic activity of the ANC nanoflakes facilitated with Ni^{2+}/Ni^{3+} and Co^{2+}/Co^{3+} redox couple at the octahedral sites of the material inline thru the oxy-functional groups. The sensor exhibited a low LOD with a wide linear range of detection covering the entire safe range of HMIs in the biological fluids and other ecological bodies like groundwater. The performance of the ANC/GCE electrode for simultaneous detection of HMI was compared with the earlier reported HMI sensors is

shown as Table 1.

3.4. PCA analysis

Generally, the overlap of the sensor response towards different HMIs leads to the complication in the abstraction of specificity of the sensor. Hence, principal component analysis (PCA) analysis was employed as the data visualization technique to confirm the spanned scatter plot distributions of the chronicled sensor response towards HMIs via the ASDPV technique. The PCA data analyzed for the detection of four heavy metal ions with ten replicates was observed with 99% original variance with three principal components (i.e., PC1 – 68.07%, PC2 – 24.32%, and PC3- 7.59%) as depicted in Fig. 3. Due to the differentiated sensitivity of the sensor towards HMIs (i.e., Cu^{2+}, Cd^{2+}, $Hg^{2+,}$ and Pb^{2+}), their fingerprints were very well distinguished via the formation of clusters in four different regions of the score plot. This distinct cluster formation of replicates of the same metals proves the eminence of simultaneous sensing. Thus, proves the excellent selectivity of the ANC/GCE towards each targeted HMIs concentration.

3.5. Mutual interference

The interference between the response of the targeted HMIs was surveyed as shown in Fig. 4. The mutual interference between the response of the sensor to Cd^{2+} - Pb^{2+} ions and Cu^{2+} - Hg^{2+} ions were examined as depicted in the Fig. S9(a, b) and S9(c, d), respectively and discussed in SI. Besides, the two analyte's mutual interference, the overall mutual interference between the four targetted HMIs was explored. In this process, the interference of Cd^{2+} ions towards the other three HMIs was examined as shown in Fig. 4(a). The Cd^{2+} concentration was varied while the concentration of other HMIs were kept constant. Here, no specific augmentation in the response of the ANC/GCE sensor was observed. Similarly, Fig. 4 (b), (c), and (d) describe the response of ANC/GCE towards constant HMI concentration with varying Cu^{2+}, $Hg^{2+,}$ and Pb^{2+} concentrations, respectively. The change in peak current for the constant HMI concentration as a response for varied metal ion concentration was observed to be less than 5% which proves the singularity and non-significant interference in the response of the ANC/GCE sensor. In contrast, the variable concentration of Hg^{2+} has a significant impact on the response of the sensor towards constant Cu^{2+} concentrations shown in Fig. 4(c), which can be due to the formation of the Hg-intermetallic layer at the surface of the electrode [8]. Though the response of the sensor towards Cu^{2+} ions increased, no specific shift in the characteristic peak or degradation in the response was observed. This proves the selectivity of the sensor towards the targeted HMI in the presence of other metallic ions.

3.6. Stability and reproducibility

The reproducibility of the ANC/GCE towards HMI sensing was examined by using five identically fabricated sensors for simultaneous determination of HMIs via ASDPV in the existence of 0.1M ABS electrolytic solution (data not shown). The relative standard deviation (RSD) value appraised for ANC/GCE concerning the response of five devices was ~2.10% (Cd^{2+}), ~3.12% (Hg^{2+}), ~3.01% (Cu^{2+}) and ~4.32% (Pb^{2+}). The aging process of the ANC/GCE was considered to estimate the reusability of the electrode (data not shown). Initially, the as-fabricated ANC/GCE electrode was employed for simultaneous determination of HMIs via the ASDPV technique and the used sensor was gently rinsed in the DI water and stored in a desiccator for 7 days. After the storage period, the same sensor was employed for the simultaneous detection of HMIs and observed with an RSD value of ~4.10% (Cd^{2+}),

Table 1
Performance comparison of ANC/GCE sensor with previously reported sensors for simultaneous sensing of HMIs.

Sensors	Procedure	Linear range of detection (ppm)		Limit of Detection (ppm)	Real- Time sample	Refs.
AFO/GCE	DPASV	Cd^{2+}	2.0×10^{-3}–2.0×10^{-1}	1.0×10^{-3}	Simulated blood serum	[8]
		Pb^{2+}	3.0×10^{-3}–3.3×10^{-1}	1.6×10^{-3}		
		Cu^{2+}	2.0×10^{-3}–2.0×10^{-1}	1.0×10^{-5}		
		Hg^{2+}	3.0×10^{-3}–3.0×10^{-1}	1.0×10^{-5}		
NiCoP-GCE	DPV	Pb^{2+}	3.0×10^{-3}–3.0×10^{-1}	1.0×10^{-4}	Groundwater	[9]
		Hg^{2+}	3.0×10^{-3}–3.0×10^{-1}	1.0×10^{-3}		
		Cd^{2+}	2.0×10^{-3}–2.0×10^{-1}	1.0×10^{-5}		
0.3(Fe_3O_4/F-MWCNT)	SWSV	Cd^{2+}	1.0×10^{-2}–7.1	3.0×10^{-3}	Tap Water	[10]
		Pb^{2+}	9.0×10^{-3}–9.9	2.8×10^{-3}		
		Hg^{2+}	4.0×10^{-3}–10.5	1×10^{-3}		
		Zn^{2+}	3.0×10^{-2}–32.5	1.2×10^{-2}		
		Cu^{2+}	1.0×10^{-2}–31.5	1.0×10^{-3}		
Cerium Hexacyanoferrate/ GCE	LSV	Cd^{2+}	2.3–2355	2.1	Water	[24]
		Pb^{2+}	3.3–3312	3.2×10^{-2}		
		Cu^{2+}	1.7–1846	1.4×10^{-1}		
		Hg^{2+}	3.2–3231	4.8×10^{-1}		
N-doped graphene / GCE	DPASV	Pb^{2+}	9.0×10^{-2}–2.3	1.3×10^{-2}	Water	[25]
		Cu^{2+}	1.0×10^{-1}–1.8	3.8×10^{-2}		
		Hg^{2+}	6.0×10^{-1} –3.2	1.3×10^{-1}		
Antimony film	ASV	Cd^{2+}	5.9–18.9	2.61×10^{-1}	-	[26]
		Pb^{2+}	8.2–26.4	9.9×10^{-2}		
Bismuth Bulk	ASV	Pb^{2+}	3.3–33.1	3.5×10^{-2}	Rain Water	[27]
		Cd^{2+}	2.0×10^{-3}–2.0×10^{-2}	1.3×10^{-2}		
F-GO/GCE	SWASV	Cd^{2+}	1.0×10^{-1}–1.1	2.0×10^{-3}	-	[28]
		Pb^{2+}	9.0×10^{-2}–1.6	3.0×10^{-3}		
Bi_2O_3 modified carbon paste	DPASV	Cd^{2+}	2.6–23.6	1.1	Water,	[29]
		Pb^{2+}	3.3–33.1	1.6	Urine	
Blast Furnace Slag	ASDPV	Pb^{2+}	3.31×10^{-2}–2.6	2.8×10^{-2}	-	[30]
		Cu^{2+}	9. $x10^{-2}$–15.00	8.3×10^{-2}		
ANC/GCE	ASDPV	Cd^{2+}	1.0×10^{-5}–1.0	1.14×10^{-6}	Drinking water,Tap water and Simulated blood serum	This work
		Pb^{2+}	1.0×10^{-5}–1.0	1.54×10^{-6}		
		Cu^{2+}	1.0×10^{-5}–1.0	2.61×10^{-6}		
		Hg^{2+}	1.0×10^{-5}–1.0	2.32×10^{-6}		

AFO-$AlFeO_3$, Bi_2O_3- Bismuth Oxide, NiCoP – Nickel Cobalt Phosphide, AA- Amino Acid, F-GO- Florine doped Graphene Oxide, F-MWCNT- Florine doped Multiwalled Carbon nanotubes, N-doped – Nitrogen-Doped, Fe_3O_4 – Iron (III) Oxide, LSV- Linear Sweep Voltammetry, ASV- Anodic Stripping Voltammetry, SWSV- Square wave Stripping Voltammetry

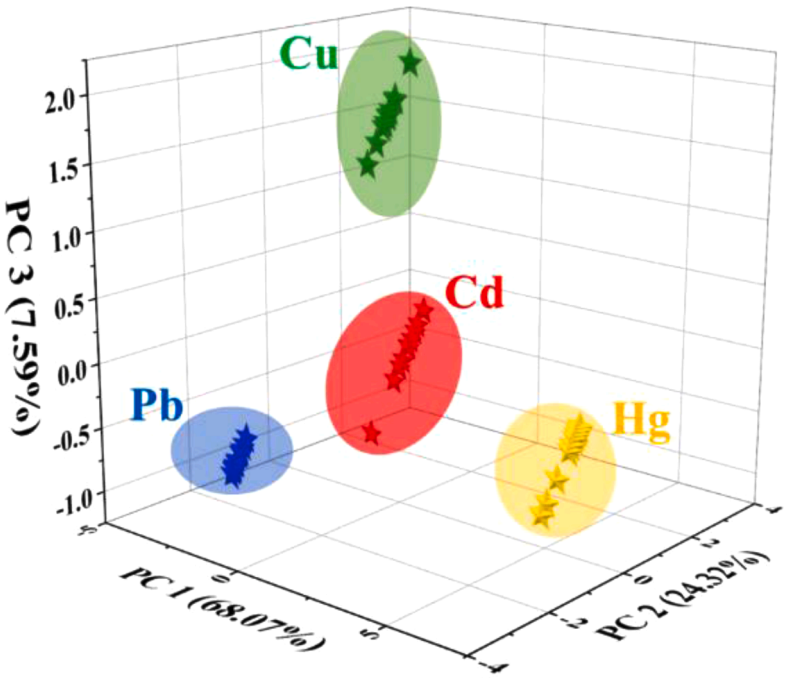

Fig. 3. PCA score plot of ANC/GCE towards simultaneous sensing of 4 different HMIs with 10 replicates.

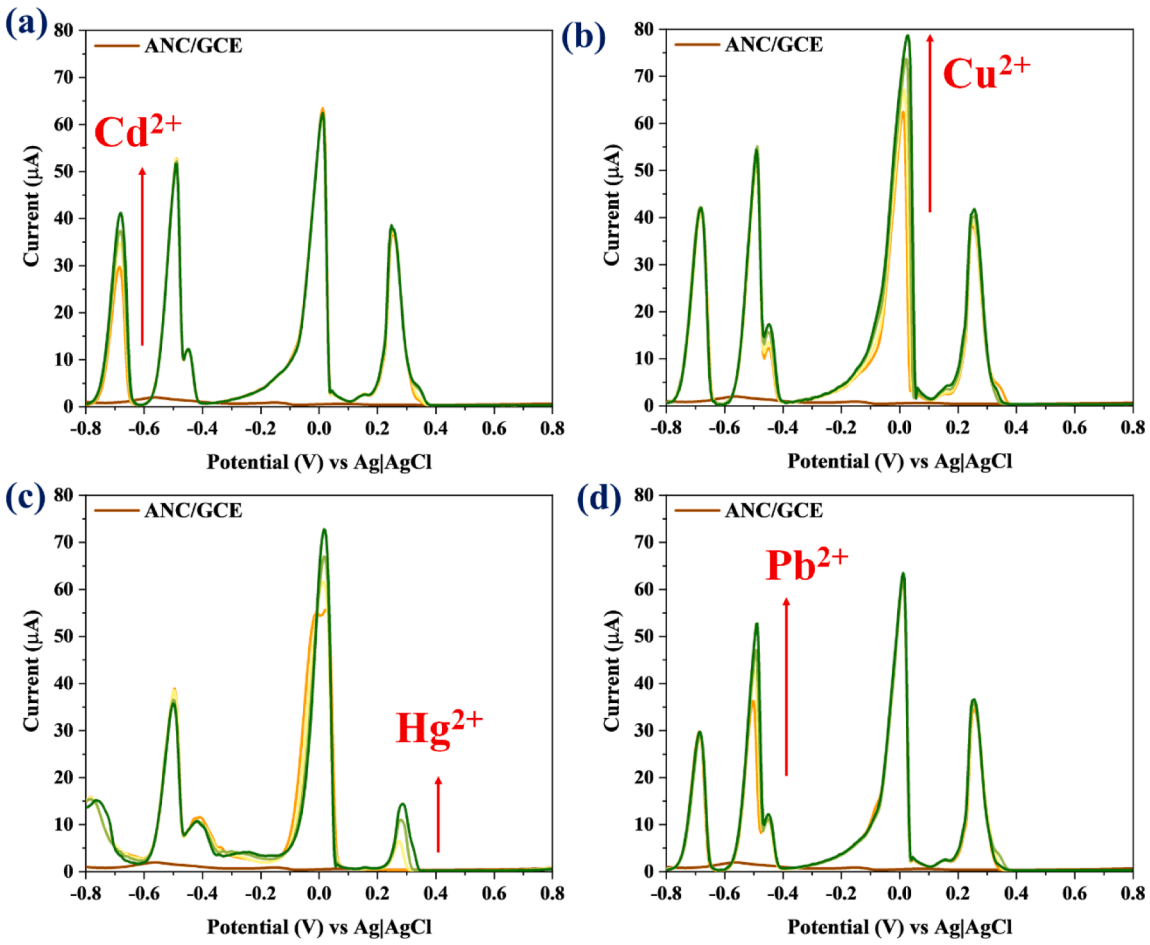

Fig. 4. Mutual interference analysis based on ASDPV response of ANC/GCE between (a) a variable Cd^{2+}, (b) a variable Cu^{2+}, (c) a variable Hg^{2+} and (d) variable Pb^{2+} with other constant HMIs concentrations.

~3.25% (Hg^{2+}), ~3.89% (Cu^{2+}), and ~4.25% (Pb^{2+}). The stability and reusability of the sensor prove it as a durable and cost-effective platform for HMI detection.

3.7. Selectivity

The major ionic constituents reported in human blood samples are Na^{+}, K^{+}, and Ca^{2+} [31]. Likewise, the tap and drinking water samples are reported with cationic constituents such as Ca^{2+}, Fe^{2+}, Mn^{2+}, Zn^{2+}, Ni^{2+}, Cr^{2+} along with Na^{+}, K^{+}, and Ca^{+} due to various reasons like rust via water distribution system, leaching of from nickel/chromium-plated taps, dezincification of brass, etc [32]. Besides, a trace level concentration of Co^{2+} is naturally found in water, soil, rock, and plants which can interfere with the sensitivity and selectivity of the HMI sensor. Hence, the selectivity of the ANC/GCE sensor towards the HMIs (i.e., Cd^{2+}-10 ppb, Pb^{2+}- 10 ppb, Cu^{2+} - 50 ppb, Hg^{2+} - 1ppb) was examined in the presence of interfering species like Na^{+}, K^{+}, Ca^{2+}, Cr^{2+}, Mn^{2+}, Fe^{2+}, Co^{2+}, Ni^{2+} and Zn^{2+} as shown in the ASDPV curve in Fig. 5(a). The corresponding change in the response of the sensor towards HMIs was analyzed as shown in Fig. S8 (a–d) in which the variation in the peak current was experiential to be less than 5%. This singularity proves the non-significant interference of the co-existing species in the response of ANC/GCE towards the targeted HMIs.

3.8. Real sample analysis

Fig. 5(b) demonstrates the ASDPV response of the ANC/GCE towards HMIs in the drinking water samples. Here we deployed the standard addition technique to evaluate the feasibility of the sensor via recovery percentages [8,9]. Fig. S10 (a–d) portrays the corresponding calibration curve with a linear regression line. The regression coefficient exhibited by the sensor towards the HMI detection was above 0.99 for all HMIs. The sensor was estimated with recovery % ranging from 99.20% to 127.13% as shown in Table S1. Likewise, the ASDPV response of ANC/GCE towards HMIs in tap water samples and simulated blood serum samples were examined as shown in Fig. 5(c) and Fig. 5(d), respectively. The corresponding calibration curves with a linear regression line is shown in Figs. S11(a–d) and S12(a–d). The sensor was assessed with recovery percentages of 99.50% to 118.84% (shown in Table S2) and from 95.44% to 126.05% (shown in Table S3) for tap water and simulated blood serum samples, respectively.

4. Conclusion

In summary, we demonstrated a one-step solid-state synthesis of ANC nanoflakes for simultaneous detection of HMIs in water and simulated blood serum samples. The ANC/GCE sensor showed a ultra-low LOD of 0.00114 ppb(Cd^{2+}), 0.00154 ppb (Pb^{2+}), 0.00261 ppb (Cu^{2+}) and 0.00232 ppb (Hg^{2+}). The PCA analysis proved the excellent selectivity of the sensor between the targeted HMIs in the medium. The ultra selectivity of sensor towards the targeted HMIs in presence of different interfering species (such as Na^{+}, K^{+}, Ca^{2+}, Cr^{2+}, Mn^{2+}, Fe^{2+}, Co^{2+}, Ni^{2+}, and Zn^{2+}) and the successful trace level determination of HMIs in tap water, drinking water, and simulated blood serum (with decent recovery percentages) proved the outstanding efficacy of the ANC/GCE sensor. The overall performance exhibited by the sensor

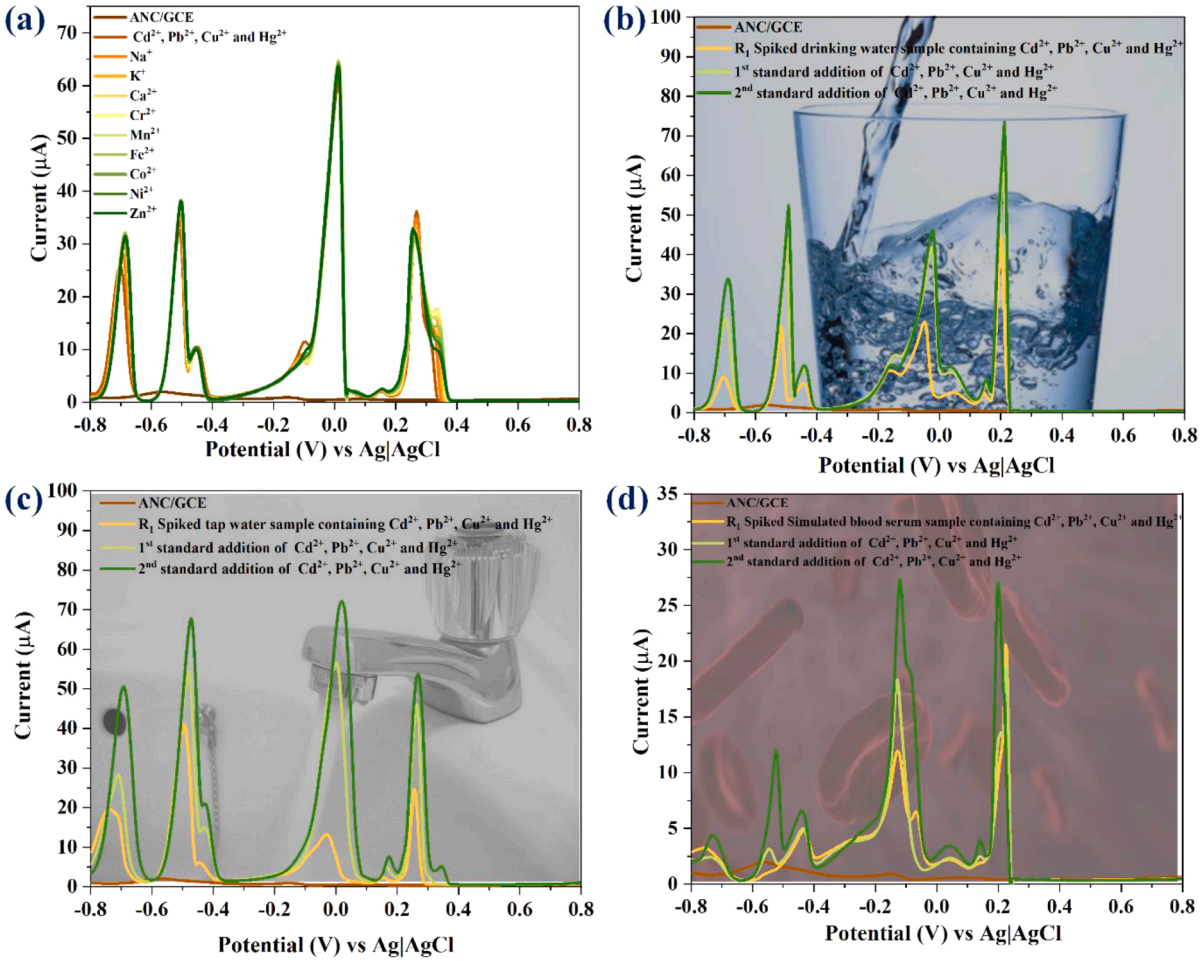

Fig. 5. (a) Selectivity analysis and real sample analysis of ANC/GCE towards HMI detection in (b) drinking water, (c) tap water and (d) simulated blood samples.

proved it as an promising platform for a variety of ecological and bio-analytical applications.

Declaration of Competing Interest

The authors declare that they have no known competing financial interests or personal relationships that could have appeared to influence the work reported in this paper.

Acknowledgments

SB acknowledges financial assistance from IIT Hyderabad Rural Development Program project no. RURDEV/2021/F135/RD02. LD acknowledges the SEM characterization facility funded by DST-FIST project No. DST-FIST (SR/FST/ETI-421/2016).

Supplementary materials

Supplementary material associated with this article can be found, in the online version, at doi:10.1016/j.snr.2022.100097.

References

[1] L. Jarup, Hazards of heavy metal contamination, Br. Med. Bull. 68 (1) (2003) 167–182, https://doi.org/10.1093/bmb/ldg032.
[2] M. Jaishankar, T. Tseten, N. Anbalagan, B.B. Mathew, K.N. Beeregowda, Toxicity, mechanism and health effects of some heavy metals, Interdiscip. Toxicol. 7 (2) (2014) 60–72, https://doi.org/10.2478/intox-2014-0009.
[3] A.L. Wani, A. Ara, J.A. Usmani, Lead toxicity: a review, Interdiscip. Toxicol. 8 (2) (2015) 55–64, https://doi.org/10.1515/intox-2015-0009.
[4] G. Genchi, M.S. Sinicropi, G. Lauria, A. Carocci, A. Catalano, The effects of cadmium toxicity, Int. J. Environ. Res. Public Health 17 (2020) 3782, https://doi.org/10.3390/ijerph17113782.
[5] F. Zahir, S.J. Rizwi, S.K. Haq, R.H. Khan, Low dose mercury toxicity and human health, Environ. Toxicol. Pharmacol. 20 (2) (2005) 351–360, https://doi.org/10.1016/j.etap.2005.03.007.
[6] W.E. Carpenter, D. Lam, G.M. Toney, N.L. Weintraub, Z. Qin, Zinc, copper, and blood pressure: human population studies, Med. Sci. Monit. 19 (2013) 1–8, https://doi.org/10.12659/MSM.883708.
[7] N. Zhang, R. Qiao, J. Su, J. Yan, Z. Xie, Y. Qiao, X. Wang, J. Zhong, Recent advances of electrospun nanofibrous membranes in the development of chemosensors for heavy metal detection, Small 13 (16) (2017), 1604293, https://doi.org/10.1002/smll.201604293.
[8] L. Durai, S. Badhulika, Simultaneous sensing of copper, lead, cadmium and mercury traces in human blood serum using orthorhombic phase aluminium ferrite, Mater. Sci. Eng. C 112 (2020), 110865, https://doi.org/10.1016/j.msec.2020.110865.
[9] L. Durai, A. Gopalakrishnan, S. Badhulika, Thermal decomposition assisted one-step synthesis of high surface area NiCoP nanosphere for simultaneous sensing of lead, mercury and cadmium ions in groundwater samples, J. Electroanal. Chem. 861 (2020), 113937, https://doi.org/10.1016/j.jelechem.2020.113937.
[10] W. Wu, M. Jia, Z. Wang, W. Zhang, Q. Zhang, G. Liu, Z. Zhang, P. Li, Simultaneous voltammetric determination of cadmium(II), lead(II), mercury(II), zinc(II), and copper(II) using a glassy carbon electrode modified with magnetite (Fe_3O_4) nanoparticles and fluorinated multiwalled carbon nanotubes, Microchim. Acta 186 (2019) 97, https://doi.org/10.1007/s00604-018-3216-5.
[11] R. Hu, X. Zhang, K.N. Chi, T. Yang, Y.H. Yang, Bifunctional MOFs-based ratiometric electrochemical sensor for multiplex heavy metal ions, ACS Appl. Mater. Interfaces 12 (27) (2020) 30770–30778, https://doi.org/10.1021/acsami.0c06291.
[12] L.A. Malik, A.H. Pandith, A. Bashir, A. Qureashi, Zinc oxide-decorated multiwalled carbon nanotubes: a selective electrochemical sensor for the detection of Pb(II) ion in aqueous media, J. Mater. Sci. Mater. Electron. (2022), https://doi.org/10.1007/s10854-022-07793-x.
[13] D. Huo, Y. Zhang, N. Li, W. Ma, H. Liu, G. Xu, Z. Li, M. Yang, C. Hou, Three-dimensional graphene/amino-functionalized metal-organic framework for simultaneous electrochemical detection of Cd(II), Pb(II), Cu(II), and Hg(II), Anal. Bioanal. Chem. 414 (2022) 1575–1586, https://doi.org/10.1007/s00216-021-03779-6.
[14] L. Chu, W. Ahmad, W. Liu, J. Yang, R. Zhang, Y. Sun, J. Yang, X.A. Li, Lead-free halide double perovskite materials: a new superstar toward green and stable optoelectronic applications, Nano Micro Lett. 11 (1) (2019) 16, https://doi.org/10.1007/s40820-019-0244-6.
[15] A.K. Hossain, M.A. Ullah, P.S. Guin, S. Roy, An overview of La_2NiMnO_6 double perovskites: synthesis, structure, properties, and applications, J. Sol Gel Sci. Technol. 93 (2020) 479–494, https://doi.org/10.1007/s10971-019-05054-8, 2020.
[16] I. T. Jolliffe, J. Cadima, Principal component analysis: a review and recent developments. Philos. Trans. Royal Soc. A, 374(2065) (201), 20150202. https://doi.org/10.1098/rsta.2015.0202.
[17] H. Hotelling, Analysis of a complex of statistical variables into principal components, J. Educ. Psychol. 24 (1933) 417–441, https://doi.org/10.1037/h0071325, 498–520.
[18] I.T. Jolliffe, Principal Component Analysis for Special Types of Data, Springer, New York, 2002, pp. 338–372.
[19] R. Bro, A.K. Smilde, Principal component analysis, Anal. Methods 6 (9) (2014) 2812–2831.
[20] L. Durai, S. Badhulika, Facile synthesis of large area pebble-like β-$NaFeO_2$ perovskite for simultaneous sensing of dopamine, uric acid, xanthine and hypoxanthine in human blood, Mater. Sci. Eng. C 109 (2020), 110631, https://doi.org/10.1016/j.msec.2020.110631.
[21] L. Durai, S. Badhulika, Highly selective trace level detection of Atrazine in human blood samples using lead-free double perovskite Al_2NiCoO_5 modified electrode via differential pulse voltammetry, Sens. Actuators B Chem. 325 (2020), 128792, https://doi.org/10.1016/j.snb.2020.128792.
[22] X. Gao, W. Wei, L. Yang, M. Guo, Carbon nanotubes/poly(1,2-diaminobenzene) nanoporous composite film electrode prepared by multipulse potentiostatic electropolymerisation and its application to determination of trace heavy metal ions, Electroanal 18 (2006) 485, https://doi.org/10.1002/elan.200503409.
[23] H. Bagheri, A. Hajian, M. Rezaei, A. Shirzadmehr, Composite of Cu metal nanoparticles-multiwall carbon nanotubes-reduced graphene oxide as a novel and high performance platform of the electrochemical sensor for simultaneous determination of nitrite and nitrate, J. Hazard. Mater. 324 (2017) 762–772, https://doi.org/10.1016/j.jhazmat.2016.11.055.
[24] B. Devadas, M. Sivakumar, S.M. Chen, M. Rajkumar, C.C. Hu, Simultaneous and selective detection of environment hazardous metals in water samples by using flower and christmas tree like cerium hexacyanoferrate modified electrodes, Electroanal 27 (11) (2015) 2629–2636, https://doi.org/10.1002/elan.201500208.
[25] Cesarino, G. Marino, J. Matos, E.G. Cavalheiro, Evaluation of a carbon paste electrode modified with organofunctionalised SBA-15 nanostructured silica in the simultaneous determination of divalent lead, copper and mercury ions, Talanta 75 (2008) 15–21, https://doi.org/10.1016/j.talanta.2007.06.032.
[26] V. Jovanovski, S.B. Hočevar, B. Ogorevc, *Ex situ* prepared antimony film electrode for electrochemical stripping measurement of heavy metal ions, Electroanal 21 (21) (2009) 2321–2324, https://doi.org/10.1002/elan.200904692.
[27] C. Armstrong, C.E. Tatum, R.N.D. Sparks, J.Q. Chambers, Z.L. Xue, Individual and simultaneous determination of lead, cadmium, and zinc by anodic stripping voltammetry at a bismuth bulk electrode, Talanta 82 (2) (2010) 675–680, https://doi.org/10.1016/j.talanta.2010.05.031.
[28] A.R. Thiruppathi, B. Sidhureddy, W. Keeler, A. Chen, Facile one-pot synthesis of fluorinated graphene oxide for electrochemical sensing of heavy metal ions, Electrochem. Commun. 76 (2017) 42–46, https://doi.org/10.1016/j.elecom.2017.01.015.
[29] R. Pauliukaite, R. Metelka, I. Švancara, A. Królicka, A. Bobrowski, K. Vytřas, K. Kalcher, Carbon paste electrodes modified with Bi_2O_3 as sensors for the determination of Cd and Pb, Anal. Bioanal. Chem. 374 (6) (2020) 1155–1158, https://doi.org/10.1007/s00216-002-1569-3.
[30] A. Mourya, S.K. Sinha, B. Mazumdar, Glassy carbon electrode modified with blast furnace slag for electrochemical investigation of Cu^{2+} and Pb^{2+} metal ions, Microchem. J. 147 (2019) 707–716, https://doi.org/10.1016/j.microc.2019.03.082.
[31] A.K. Covington, R.A. Robinson, References standards for the electrometric determination, with ion-selective electrodes, of potassium and calcium in blood serum, Anal. Chim. Acta 78 (1) (1975) 219–223, https://doi.org/10.1016/s0003-2670(01)84768-1.
[32] F. Edition, Guidelines for Drinking-Water Quality, 38, WHO Chronicle, 2011, pp. 104–108.